



# Design and Application of an S-band Fast Radio Bursts Search Pipeline for the Nanshan 26m Radio Telescope

Yan-Ling Liu<sup>1,2</sup>, Mao-Zheng Chen<sup>1,2</sup>, Jian Li<sup>1,2</sup>, Jian-Ping Yuan<sup>1</sup>, Rai Yuen<sup>1</sup>, Zhi-Yong Liu<sup>1</sup>, Hao Yan<sup>1,2</sup>, Wen-Long Du<sup>1,3</sup>, and Nan-Nan Zhai<sup>1,3</sup>

<sup>1</sup> Xinjiang Astronomical Observatory, Chinese Academy of Sciences, Urumqi 830011, China; [liuyanling@xao.ac.cn](mailto:liuyanling@xao.ac.cn)

<sup>2</sup> Xinjiang Key Laboratory of Microwave Technology, Urumqi 830011, China

<sup>3</sup> University of Chinese Academy of Sciences, Beijing 100049, China

Received 2024 April 11; revised 2024 May 16; accepted 2024 May 30; published 2024 July 8

## Abstract

Fast radio bursts (FRBs) are among the most studied radio transients in astrophysics, but their origin and radiation mechanism are still unknown. It is a challenge to search for FRB events in a huge amount of observational data with high speed and high accuracy. With the rapid advancement of the FRB research process, FRB searching has changed from archive data mining to either long-term monitoring of the repeating FRBs or all-sky surveys with specialized equipments. Therefore, establishing a highly efficient and high quality FRB search pipeline is the primary task in FRB research. Deep learning techniques provide new ideas for FRB search processing. We have detected radio bursts from FRB 20201124A in the *L*-band observational data of the Nanshan 26 m radio telescope (NSRT-26m) using the constructed deep learning based search pipeline named dispersed dynamic spectra search (DDSS). Afterwards, we further retrained the deep learning model and applied the DDSS framework to *S*-band observations. In this paper, we present the FRB observation system and search pipeline using the *S*-band receiver. We carried out search experiments, and successfully detected the radio bursts from the magnetar SGR J1935+2145 and FRB 20220912A. The experimental results show that the search pipeline can complete the search efficiently and output the search results with high accuracy.

*Key words:* radio continuum: general – methods: data analysis – methods: observational

## 1. Introduction

Fast radio bursts (FRBs) are bright, highly dispersed, and millisecond-duration cosmological radio transients (see Lorimer et al. 2007; Cordes & Chatterjee 2019; Petroff et al. 2019). Nearly 800 FRB sources have been reported since the transient radio phenomenon was first detected in 2007, and most are non-repeating, while only 65 are known repeaters.<sup>4</sup> Most repeating FRBs were detected only twice. The study of FRBs has entered a new era as the active periods of several repeating FRBs have been captured, such as FRB 20121102 (Cruces et al. 2021), FRB 20180916B (Chen et al. 2021), and FRB 20201124A (Xu et al. 2022). This has resulted in a collection of a large number of radio burst samples, which helps to study their respective energy distributions, polarization properties, and time-dependent properties. However, their physical origin and radiation mechanism are still unknown, and we still need more FRB samples for analysis and study.

The establishment of an efficient FRB search pipeline is of great significance for voltage data dump, improving the speed and accuracy for observation data processing and carrying out

FRB follow-up observations in time. As early as 2016, the Nanshan 26 m radio telescope (NSRT-26m) conducted FRB blind search observations in the *L*-band. Afterwards, we upgraded the digital terminal system and developed a deep learning based search pipeline named dispersed dynamic spectra search (DDSS) in 2022, which successfully detected radio bursts in the data of targeted search for repeating FRB 20201124A using *L*-band receiver (Liu et al. 2022). The application of deep learning techniques in FRB observation search has greatly improved the search accuracy. But the performance of a deep learning based classifier greatly depends on the quality of training samples. When applying the DDSS pipeline to the *S*-band, the deep learning model needs to be retrained, and the radio frequency interference (RFI) mitigation method also needs to be redesigned. In this paper, an FRB observation system and a search pipeline are built, which are deployed to search for the radio bursts from magnetar SGR J1935+2154 and FRB 20220912A at *S*-band using the NSRT-26m. The rest of this paper is organized in the following manner. In Section 2, we describe the observing system. The third section describes the search pipeline, and the fourth section describes our observation experiment and the results. We present our conclusions in Section 5.

<sup>4</sup> <https://blinkverse.alkaidos.cn/>

## 2. Observation System

### 2.1. Receiver System

The NSRT-26m is located at E87°10.67', N43°28.27' at an altitude of 2080 m, and is operated by Xinjiang Astronomical Observatory (XAO) of Chinese Academy of Sciences (Wang et al. 2001). The telescope is equipped with *L*-band, *C*-band, *S*/*X* band, *K*-band, and *Q*-band receivers. According to the current state of FRB observation, FRBs are mainly detected at radio frequencies between 110 MHz (FRB 20180916B, Pleunis et al. 2021) and 8 GHz (FRB 121102, Gajjar et al. 2018). Of course, this is mainly due to the limited frequency range of the observation equipments. The Low Frequency Array (LOFAR) detected FRBs at the lowest frequencies to date, with observation frequencies ranging between 110 and 188 MHz (Pleunis et al. 2021). The NSRT-26m can conduct FRB observations in the *L*-band, *S*-band, and *C*-band. In 2022 February and March, we detected radio bursts from FRB 20201124A with the *L*-band receiver.

In 2022 August, the *L*-band observations were discontinued at the NSRT-26m due to upgrades on the *L*-band receiver. Since then, we have been using the room-temperature *S*-band receiver, with 60 K system temperature, for FRB observations. The frequency range for the *S*-band is from 2.1 to 2.6 GHz, with a bandwidth of 500 MHz. Because of the RFI effects, the radio frequency (RF) front end of the *S*-band receiver is partly filtered, such that the actual observed frequencies are from 2182 to 2382 MHz. We use the radiometer equation (see, e.g., Lorimer & Kramer 2005) to compute the minimum detectable fluence

$$F_{\min} = \frac{T_{\text{sys}} S/N}{G} \sqrt{\frac{W_{\text{obs}}}{BN_p}} \quad (1)$$

where  $G = \frac{A\eta}{2k}$  is the gain of NSRT-26m, and  $\eta = 47\%$  is the aperture efficiency,  $A$  is the aperture area, and  $k$  is the Boltzmann's constant. In addition,  $N_p = 2$  is the number of summed polarizations,  $B = 200$  MHz is the effective observing bandwidth, and  $T_{\text{sys}} = 60$  K is the system temperature. We assume the minimum FRB pulse width  $W_{\text{obs}} = 1$  ms, and a signal-to-noise ratio (S/N) threshold of 10. From this, we obtain  $F_{\min} \approx 10.5$  Jy ms for the *S*-band receiver.

### 2.2. Digital Backend

The digital backend for FRB observations is based on the Reconfigurable Open Architecture Computing Hardware 2 (ROACH2) board<sup>5</sup> with frequency bandwidth of 512 MHz and is independently developed by XAO, referred to as the XAO FilterBank (XFB) system. Its time resolution is 64  $\mu$ s and frequency resolution can be set to either 0.5 MHz or 1 MHz. The observation data are packaged in the Flexible Image

Transport System (FITS) format and can be converted to filterbank format as needed.

After the astronomical signal is reflected by the single-dish telescope, it enters the receiver system, where it is converted into two intermediate frequency (IF) signals, A and B, through a polarizer, followed by multistage amplification, filtering and mixing. The two analog-to-digital converters (ADCs) in the XFB perform high-speed sampling of the two IF signals A and B, respectively. After that, multiple operations such as filtering, fast Fourier transform (FFT), Stokes parameter calculation, and data packaging will be done based on the Field Programmable Gate Array (FPGA) module. Lastly, the signal data are transferred to the high-performance computing (HPC) platform through 10 Gigabit Ethernet (10 GbE). The main work of the HPC includes putting the data transmitted from the 10 GbE network into the first-input first-output (FIFO) buffer, packaging the data in PSRFITS format and finally storing the data on the hard disk. The data are then processed by the FRB search pipeline based on the deep learning technique. The *S*-band FRB observation and processing framework on the NSRT-26m are illustrated in Figure 1.

## 3. The Search Pipeline

### 3.1. Pipeline Design

For the traditional single-pulse search method, the key processing is the dedispersion algorithm, e.g., heimdall (Barsdell et al. 2012), presto (Ransom 2001), etc. For the blind FRB search, it is necessary to carry out the dispersion with dispersion measure (DM) trials and calculate the S/N for each dedispersed time series. The dedispersion processing of multiple DMs is a resource-intensive and time-consuming process. Meanwhile, in order not to miss rare FRB events, the detection S/N threshold is usually set very low. This raises the challenges of noise and RFI masquerading as false positives. In order to improve the processing accuracy and speed, deep learning techniques are applied to the procedures for processing the FRB observational data. Currently, there are two main technical routes as depicted in Figure 2. The first route is to search directly for single pulse events in the observational data with deep learning classifiers without relying on any traditional search algorithm (e.g., Zhang et al. 2018; Liu et al. 2022), and the second route involves applying a deep learning classifier to classify the candidates generated by the search software based on the traditional dedispersion algorithm (e.g., Connor & van Leeuwen 2018; Agarwal et al. 2020).

In this paper, we use the DDSS pipeline based on the technical route 1 for processing FRB observational data. The specific process flow is shown in Figure 3. The filterbank data were cut into frames of 2048 samples each along the time axis, which are in the form of the dynamic spectrograms. They are preprocessed before being fed into the deep learning classifier. The preprocessing operation mainly includes RFI mitigation,

<sup>5</sup> [https://casper.berkeley.edu/wiki/ROACH2\\_Revision\\_2](https://casper.berkeley.edu/wiki/ROACH2_Revision_2)

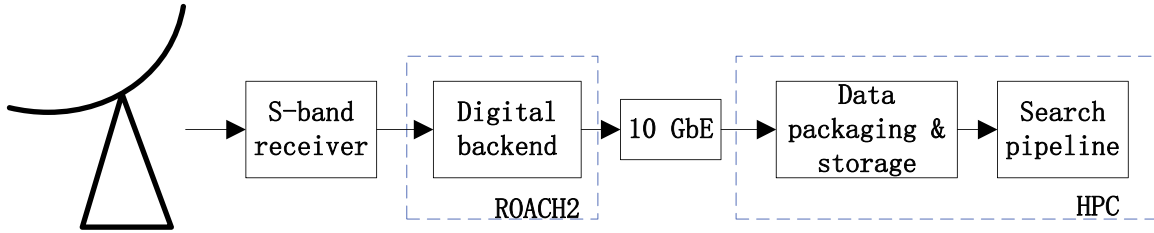


Figure 1. The S-band FRB observation and processing framework on the NSRT-26m.

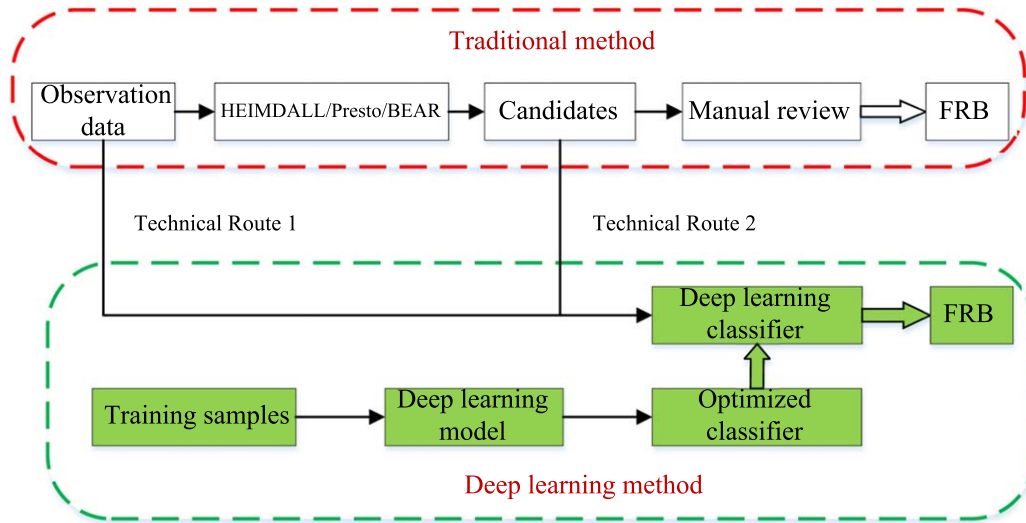


Figure 2. The technical routes of FRB search pipeline.

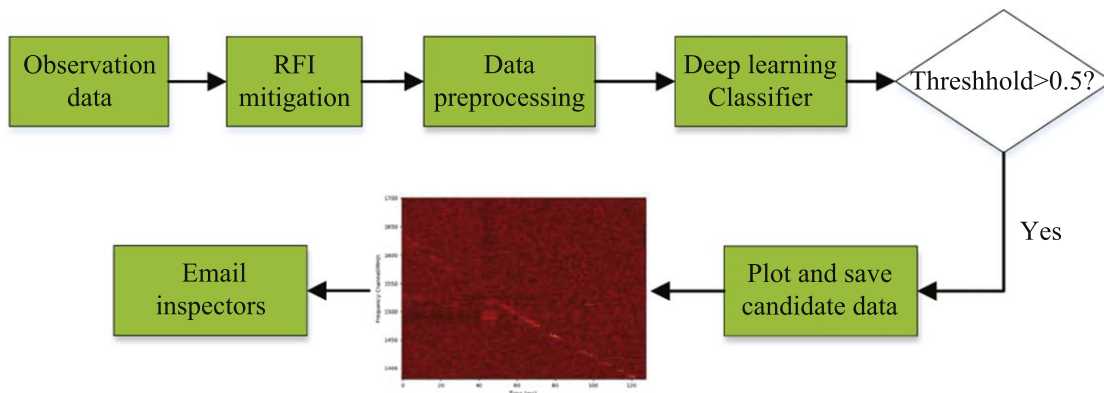
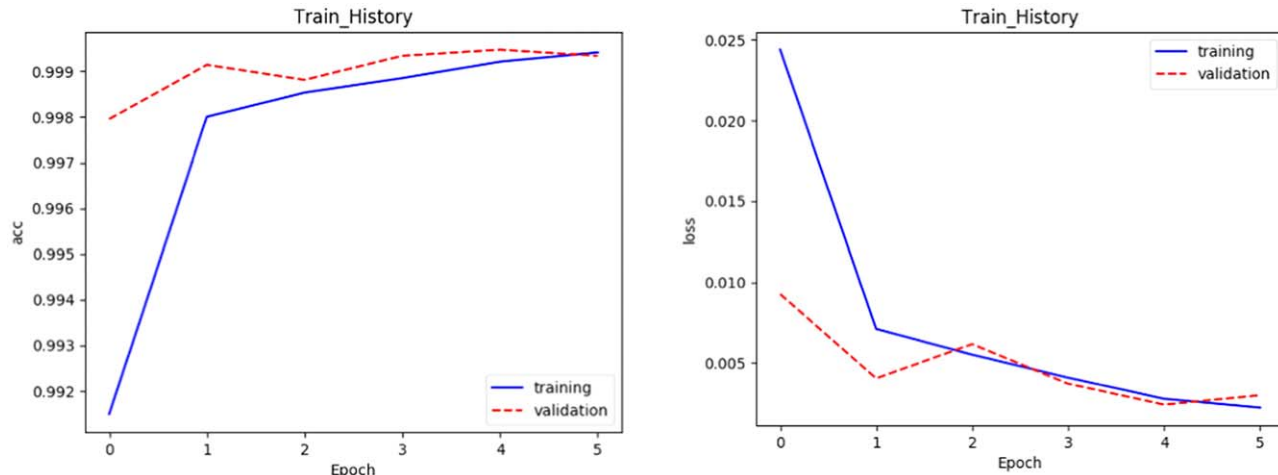


Figure 3. The flow chart of DDSS pipeline (Liu et al. 2022).

trimming, down-sampling and so on. When the prediction score of one sample is above 0.5, it is considered as an FRB. The pipeline will save the frequency-time image of the FRB candidate on the hard disk for offline visual inspection and inform the observers by email. More details of the pipeline are given by Liu et al. (2022).

When the pipeline is applied to the S-band observation data, we need to retrain the deep learning model to obtain a new deep learning classifier. We selected Xception as the deep learning network model, and utilized the simulation method to generate FRB samples as positive samples with DM ranging between 200 and 500 pc cm<sup>-3</sup>. The negative samples are all randomly



**Figure 4.** Accuracy and loss change curves with epoch of the Xception model training process on both training and validation data sets.

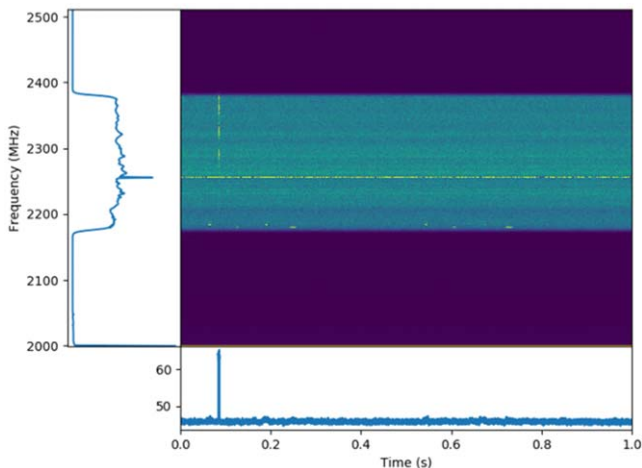


**Figure 5.** Dynamic spectrum of S-band observation data.

extracted from the real observational data without single pulses. A training set of 60,000 samples was prepared. The training was carried out on an Nvidia GTX 1080 GPU card and lasted for about 1.5 hr with 6 epochs. We conducted several model training experiments, and the model training precision, accuracy, and recall were all achieved above 98%. Figure 4 features the accuracy and loss curves for training and validation subsets with epoch of the training process. The results show that, using only 6 epochs for training, the Xception model achieved very high performance on the classification task.

RFI in observational data can have a large impact on the training performance of deep learning models. In particular, some significant RFIs can even become the learning focus of a deep learning network model. When we analyzed the S-band observation data, we found that the quality of the data is

better than that at the L-band showing only some narrowband RFIs and sporadic transient broadband RFIs, as depicted in Figure 5. Therefore, we have simplified the RFI mitigation process for the DDSS pipeline to only zapping the RFI channels. The processing speed of the pipeline is dramatically increased to more than six times the speed of data generation, which is fast enough to conduct real-time observational search missions.

### 3.2. Pipeline Test

Based on our past experience in applying the DDSS pipeline in the L-band, in this paper we do not perform further testing and validation work, but directly use the trained network model for FRB search in the S-band observations. A search experiment for the S-band search pipeline was conducted on approximately 4.6 hr of data observed on 2022 October 26. The pipeline returned only 47 false-positive candidates, most of which were caused by transient broadband RFIs, as shown in Figure 6.

Although such an error rate is acceptable, a higher search accuracy is desired given the need to store raw voltage data. Therefore, optional handling of such broadband transient RFI has been added to the search pipeline. The zero-DM matched filter (ZDMF) proposed by Men et al. (2019) was used as the mitigation strategy for broadband RFI to further improve the search accuracy of the pipeline. In practice, the RFI mitigation methods can be selected and set as necessary for a specific search task. The specific experimental data are shown in Table 1. It can be seen that the application of ZDMF further improves the accuracy of search pipeline, but the processing time increases accordingly. It is worth noting that since the execution speed of the developed software is related to the hardware platform used, the programming language, the degree

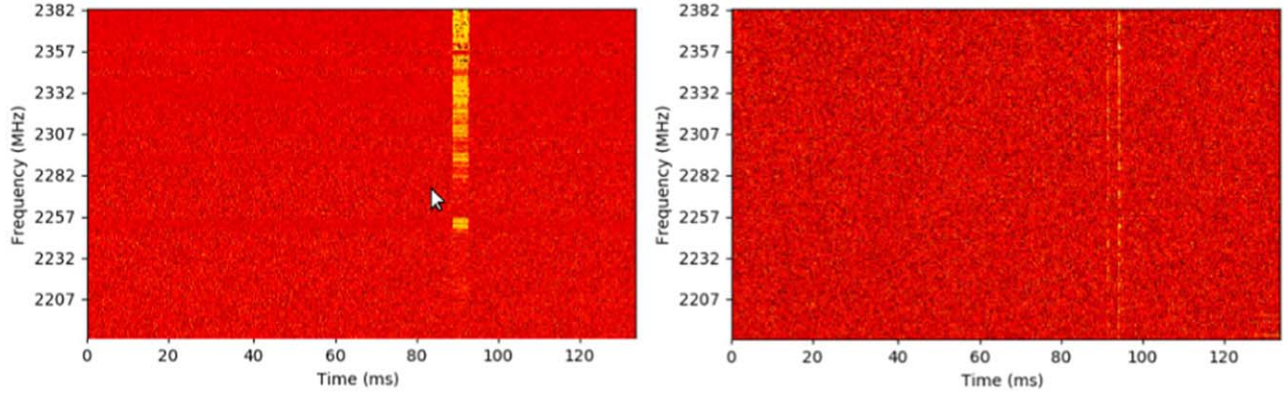


Figure 6. False positive candidates output from S-band search pipeline.

Table 1

The Execution Speed of the RFI Mitigation Algorithm and the Number of False Positive Candidates Produced by the FRB DDSS Pipeline

Method	Observation Duration (hr)	Processing Time (hr)	False Detections
Zapping	4.65	0.56	47
Zapping + ZDMF		6.39	15

Table 2

Fast Radio Bursts Emanating from SGR J1935+2154 Reported in this Paper

Event UTC	S/N	DM ( $\text{pc cm}^{-3}$ )
2022-11-20 10:35:52.311936	40.85	330
2022-11-20 10:35:52.232064	77.32	
2022-11-20 10:35:53.229440	6.0	
2022-11-20 10:35:53.491584	7.03	

of code optimization, etc., it makes more sense to make relative comparisons of speed here, and the absolute speed can only be used as a reference.

## 4. Search Experiment

### 4.1. SGR J1935+2154

In 2021, FRB 200428 was confirmed as originating from the galactic magnetar SGR J1935+2154 (Li et al. 2021). This was a landmark development as it proved that magnetars can be a physical origin of FRBs. On 2022 October 14, the Gravitational-wave High-energy Electromagnetic Counterpart All-sky Monitor (GECAM) detected an X-ray burst associated with an FRB, and scientists quickly confirmed that it originated from the magnetar SGR J1935+2154 (Wang et al. 2022). This was the second time that the high-energy counterpart of an FRB was detected. The NSRT-26m then began to conduct follow-up observations of FRB 200428, and fortunately based on the S-band search pipeline described in this paper, the radio bursts from the magnetar SGR J1935+2154 were found in the observation conducted on 2022 November 20. Dedispersed pulses and dynamic spectra of the bursts from FRB 200428 with a DM of  $330 \text{ pc cm}^{-3}$  are shown in Figure 7, and specific information for the bursts is displayed in Table 2.

Table 3

Fast Radio Bursts Emanating from FRB 20220912A Reported in this Paper

Event UTC	S/N	DM ( $\text{pc cm}^{-3}$ )
2022-10-29 15:11:39	5.3	220
2022-11-16 20:52:37	7.25	

### 4.2. FRB 20220912A

FRB 20220912A is a highly active repeating FRB detected by the Canadian Hydrogen Intensity Mapping Experiment (CHIME) in the fall of 2022, and the FRB remained highly active for several months. Twelve bursts from FRB 20220912A were detected by CHIME in the 400–800 MHz band between 2022 September 12 and October 15 (McKinven & Chime/Frb Collaboration 2022), with the brightest burst possessing a DM of  $219.46 \text{ pc cm}^{-3}$ . FRB 20220912A was subsequently detected by FAST in the 1000–1500 MHz band (Zhang et al. 2022), and by the Arecibo 12 m radio telescope at 2.3 GHz (Perera et al. 2022). Two radio bursts with low S/N from FRB 20220912A in the NSRT-26m observations were identified using the S-band FRB search pipeline. The dedispersed pulses and dynamic spectra of the two bursts with a DM of  $220 \text{ pc cm}^{-3}$  are shown in Figure 8, and their specific information is displayed in Table 3.

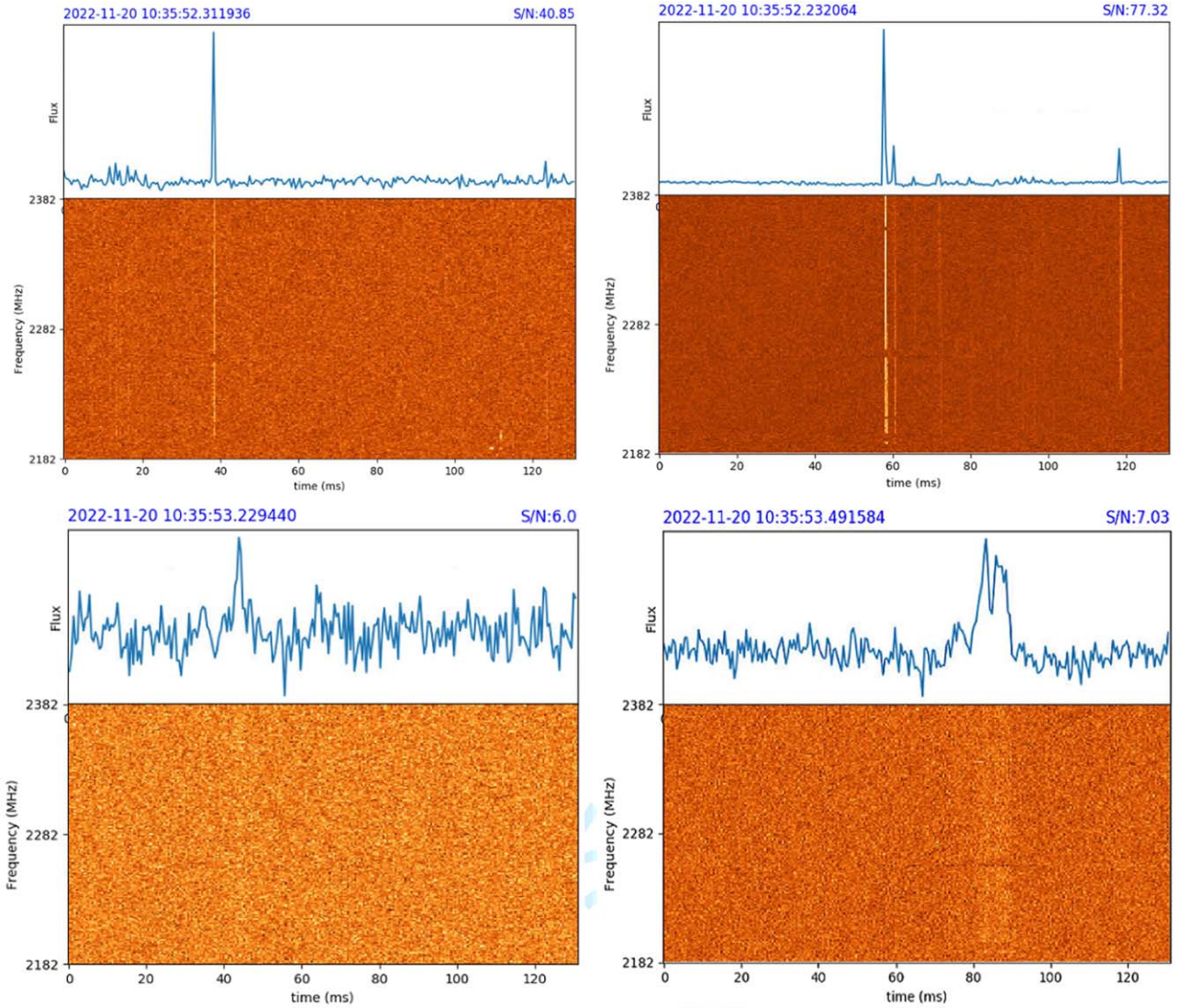


Figure 7. Bursts from SGR J1935+2154 in the S-band observational data.

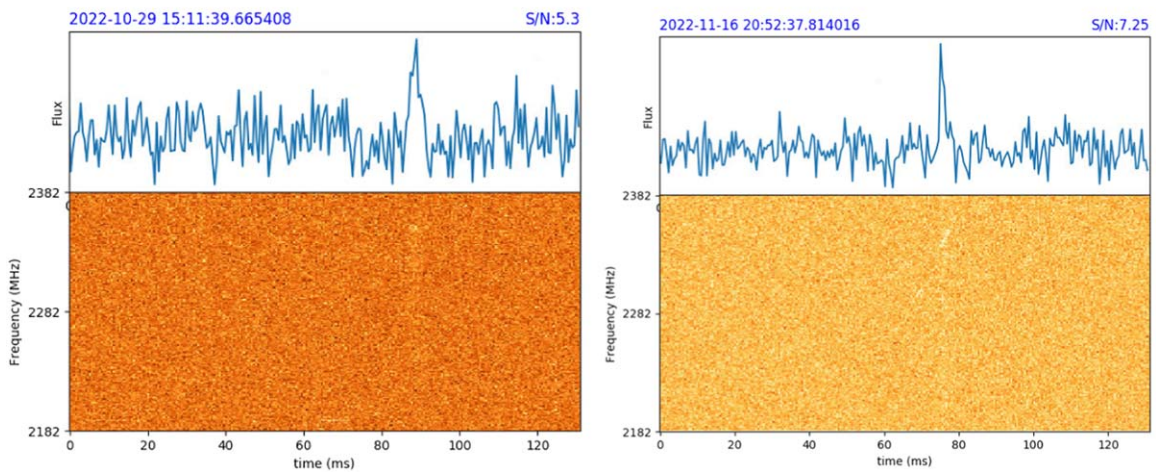


Figure 8. The two bursts from FRB 20220912A in the S-band observational data.

## 5. Conclusions

We have established an FRB search pipeline based on the FRB DDSS pipeline for the *S*-band observation data obtained from the NSRT-26m. Given that the RFI situation in the *S*-band observation data is simpler than that in the *L*-band, only two layers of RFI mitigation procedure are adopted, which are narrowband RFI zapping and ZDMF for broadband RFI. We also carried out experiments on the processing speed of the search pipeline for different RFI mitigation procedures. The results from the experimental data support the real-time searching of the FRB dynamic spectra. Using the *S*-band DDSS pipeline, the FRB observational search data obtained from October to November by the NSRT-26m were processed. We detected the radio bursts from magnetar SGR J1935+2154 and FRB 20220912A, which further demonstrated the applicability and practicability of the DDSS pipeline framework.

## Acknowledgments

We appreciate the referee for valuable comments which improved the presentation of the paper. This work is supported by the Chinese Academy of Sciences (CAS) “Light of West China” Program (No. 2022-XBQNXZ-015), the National Natural Science Foundation of China (NSFC, grant No. 11903071) and the Operation, Maintenance and Upgrading

Fund for Astronomical Telescopes and Facility Instruments, budgeted from the Ministry of Finance (MOF) of China and administered by the Chinese Academy of Sciences (CAS).

## References

- Agarwal, D., Aggarwal, K., Burke-Spolaor, S., Lorimer, D. R., & Garver-Daniels, N. 2020, *MNRAS*, **497**, 1661
- Barsdell, B. R., Bailes, M., Barnes, D. G., & Fluke, C. J. 2012, *MNRAS*, **422**, 379
- Chen, H. Y., Gu, W. M., Sun, M. Y., Liu, T., & Yi, T. 2021, *AJ*, **921**, 147
- Connor, L., & van Leeuwen, J. 2018, *AJ*, **156**, 256
- Cordes, J. M., & Chatterjee, S. 2019, *ARA&A*, **57**, 417
- Cruces, M., Spitler, L. G., Scholz, P., et al. 2021, *MNRAS*, **500**, 448
- Gajjar, V., Siemion, A. P. V., Price, D. C., et al. 2018, *AJ*, **863**, 2
- Li, C. K., Lin, L., Xiong, S. L., et al. 2021, *NatAs*, **5**, 378
- Liu, Y. L., Li, J., Liu, Z. Y., et al. 2022, *RAA*, **22**, 105007
- Lorimer, D. R., Bailes, M., McLaughlin, M. A., Narkevic, D. J., & Crawford, F. 2007, *Sci*, **318**, 777
- Lorimer, D. R., & Kramer, M. 2005, *Handbook of Pulsar Astronomy* (Cambridge: Cambridge Univ. Press), 19
- McKinven, R. & Chime/Frb Collaboration 2022, *ATel*, **15679**, 1
- Men, Y. P., Luo, R., Chen, M. Z., et al. 2019, *MNRAS*, **488**, 3957
- Perera, Benetge, Perillat, et al. 2022, *ATel*, **15734**, 1
- Petroff, E., Hessels, J. W. T., & Lorimer, D. R. 2019, *A&ARv*, **27**, 4
- Pleunis, Z., Michilli, D., Bassa, C. G., et al. 2021, *ApJL*, **911**, L3
- Ransom, S. 2001, *New Search Techniques for Binary Pulsars*, Thesis, Harvard
- Wang, C. W., Xiong, S. L., & Zhang, Y. 2022, *ATel*, **15682**, 1
- Wang, N., Wu, X. J., Manchester, R. N., et al. 2001, *ChJAA*, **1**, 195
- Xu, H., Niu, J. R., Chen, P., et al. 2022, *Natur*, **611**, E12
- Zhang, Y. K., Niu, J. R., Feng, Y., et al. 2022, *ATel*, **15733**, 1
- Zhang, Y. G., Gajjar, V., Foster, G., et al. 2018, *AJ*, **866**, 149